INVERSE CRS

H. Perroud, M. Tygel, and L. Freitas

email: *mtygel@gmail.com*
keywords: *CRS, amplitudes, inverse*

ABSTRACT

The CRS method is a powerful tool to produce high-quality stacked images of multi-coverage seismic data. As a result of the application of CRS, not only a stacked section, but also a number of attributes defined at each point of that section, are produced. In this way, one can think of the CRS application as a transformation from data space to attribute space. However, as the CRS method is purely kinematic, it should be completed by amplitude information, that we propose to obtain from the zero-offset (ZO) section and common midpoint (CMP) gather. In this paper, we propose an algorithm for an (approximate) Inverse CRS transformation, namely one that (approximately) transforms the CRS attributes back to data space. The CRS transform pair established in this way may find a number of applications in seismic imaging and data processing, in the same way as other well-known transformations, e.g., Fourier, Radon, tau-p, etc.

INTRODUCTION

CRS (Common Reflection Surface) is a recent data-driven time imaging process (see, e.g., Hubral, 1999; Jäger et al., 2001) and also references therein) that has been originally proposed as an alternative to the classical NMO-DMO chain (see, e.g., Yilmaz, 2000) to build seismic stacked, zero-offset (ZO) time images of the subsurface. As already discussed elsewhere (see, e.g., Perroud and Tygel, 2005), the CRS method has both advantages and disadvantages with respect to its competitors. In fact, the adoption of the CRS method by the geophysical community has been until now only limited, because the classical NMO-DMO chain already provides good-quality robust results, so the need for a change is not obvious.

However, CRS does not provide only zero-offset images, but also a set of wavefield attributes (emergence angles and wavefront curvatures) that have been exploited in several applications. These include, e.g., velocity model building (Della-Moretta et al., 2001; Klüver, 2006), multiple attenuation (Prüssmann et al., 2006), residual statics correction, (Koglin et al., 2006), among others.

CRS can be seen as a transformation from the data space (seismic amplitudes as a function of position and time) into attribute space (wavefield attributes as a function of position and time). Note that data space position variables include both midpoint and offset coordinates, while the attribute space position variables consist in the midpoint coordinates only. In this way, the attribute domain is much smaller, even if several attributes exist per mid-point. This transformation can thus be represented by the equation

$$\{\mathcal{D}(t,m,h)\} \stackrel{CRS}{\Longrightarrow} \{\mathcal{A}(t,m)\}\ , \tag{1}$$

where $\mathcal{D}(t,m,h)$ and $\mathcal{A}(t,m)$ denote the data and attribute sets, respectively. Also, t denotes time, m midpoint position and h half-offset.

The CRS method provides also a generalized hyperbolic moveout expression that allows for travel-time estimations for reflection event at any midpoint and offset in the vicinity of a reference position where the attributes have been estimated. For example, in the 2D case, the number of CRS attributes is three. Assuming that these attributes, denoted by A_1, A_2 and A_3, were estimated at mid-point position $m = 0$ and

at time $t(0,0)$, the traveltime, $t(m,h)$, for a reflection at midpoint m and half-offset h can be approximated as

$$t^2(m,h) = (t(0,0) + A_1 m)^2 + A_2 m^2 + A_3 h^2 \tag{2}$$

The above representation of the data in the new (attribute) domain is not complete, since it is purely kinematic. We miss the amplitude of the seismic events, that are necessary for a full representation of the data. In this sense, it can be stated that the CRS transformation, on its own, induces a loss of information that cannot be reversed. To establish a transformation that could allow to go back from the attribute space to the data space, we need to add some dynamic information. Our purpose here is to demonstrate that this goal can be achieved if we have, in addition to the CRS attributes at a given trace, also data from two trace gathers in its vicinity. These are (1) the real-amplitude (as if measured) ZO gather and (2) the CMP gather centered at the reference midpoint. The chosen ZO and CMP traces should be sufficiently close to the reference midpoint, so that the validity of the CRS approximation of any reflection traveltime is valid in this range. We propose then to call Inverse CRS this new transformation, that could be represented by the equation (compare with equation 1)

$$\{\mathcal{A}(t,0), \mathcal{D}(t,m,0), \mathcal{D}(t,0,h)\} \overset{InverseCRS}{\Longrightarrow} \{\mathcal{D}(t,m,h)\}\,, \tag{3}$$

where $\mathcal{A}(t,0)$ is the CRS attribute set at the reference midpoint, and $\mathcal{D}(t,m,0)$ and $\mathcal{D}(t,0,h)$ are the ZO and CMP data sets, respectively. Since the (forward) CRS transformation of equation 1 is essentially an approximate process (namely, it is realized upon the use of the hyperbolic travel-time approximation 2), the proposed Inverse CRS transformation of equation 3 should also not be expected to provide exact (loss-free) results. One of our goal is therefore to evaluate in which range these losses can be considered as insignificant.

It is to be remarked that a real-amplitude ZO section is not easily available in seismic exploration. As a consequence, to implement the CRS inverse transformation, we need to assume that the ZO section is available[1]. A discussion on how to obtain a valid approximation of the real-amplitude ZO section from the multicoverage data, that can be used for our inverse CRS transformation purposes, lies outside the scope of the present paper. Here we only observe that such ZO section can, in principle, be obtained together with the CRS attributes and an adequate average of the available, near-offset traces. An algorithm to actually perform this task is a topic of further investigation.

In the following, we describe the Inverse CRS transformation, as well as the algorithm that allows one to build a trace at any midpoint and offset. As indicated above, both the ZO and CMP sections in the vicinity of the reference trace are assumed to be available. For illustrative purposes, we apply it to two simple synthetic cases of a dipping planar and a circular reflector. Finally, our algorithm have been tested for the interpolation of missing traces in a real high-resolution seismic dataset.

THE INVERSE CRS TRANSFORMATION

The problem to be solved can be formulated as follows: to build the unknown data trace at a given midpoint position and offset, in the vicinity of a reference trace, for which we know (a) the CRS attributes, (b) the ZO gather and (c) the CMP gather. The known ZO and CMP gathers consists of traces located in the vicinity of the reference trace.

The construction of the unknown data trace means filling the “right" amplitude (i.e., a valid approximation of it) at all time samples. We therefore need to estimate both time and amplitude for all events that can be identified in the known part of the data. We shall describe below how these are estimated. As far as possible, we want this transformation to be macro-model independent, so we shall try to use in the process data-related quantities only.

Equation for travel-time

Travel-time estimation can be achieved directly using the CRS travel-time approximation, like the one shown above in equation 2 for the 2D case. For an event such that the ZO travel-time at the reference point

[1]We remark, in passing, that the Inverse CRS transformation is not restricted to seismic data. For GPR data, for example, this drawback is overcome since a fairly close approximation to the ZO section can be obtained from measurements using shielded antennas.

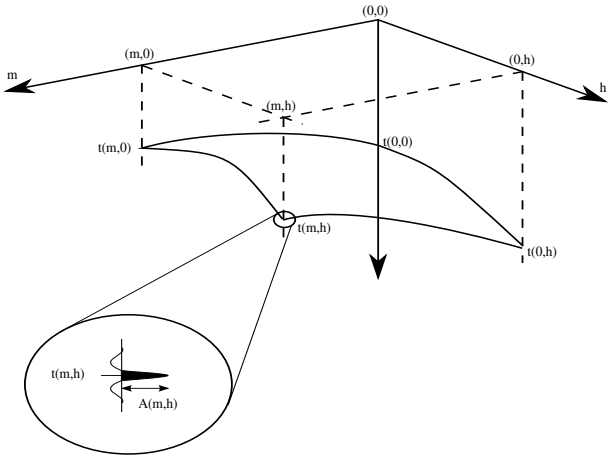

Figure 1: Schematic representation of quantities used in the calculation

is $t(0,0)$, we can evaluate the corresponding travel-time at any neighboring position m and half-offset h, since the CRS attributes are known at the reference trace (located at midpoint $m = 0$). However, it could be helpful in practice to decompose the calculation into the three steps below. The reason is that we shall make use later of the calculated values obtained in the individual steps.

- First, we evaluate $t(0,h)$, the time of the chosen event within the CMP gather, at half-offset h. In the 2D case, this is obtained setting $m = 0$ in equation 2, namely

$$t^2(0,h) = t(0,0)^2 + A_3 h^2. \tag{4}$$

- Second, we evaluate $t(m,0)$, the travel-time of the chosen event within the ZO section, at midpoint m. In the 2D case, this is obtained setting $h = 0$ in equation 2, namely

$$t^2(m,0) = (t(0,0) + A_1 m)^2 + A_2 m^2. \tag{5}$$

- Finally, we evaluate $t(m,h)$, the travel-time for the same event at mid-point m and half-offset h. This can be achieved by means of the equation

$$t^2(m,h) = t(m,0)^2 + t(0,h)^2 - t(0,0)^2, \tag{6}$$

  which combines the previous two results.

This final equation 6 reveals how the travel-time of a reflection event at any midpoint and offset can be simply derived from the ones that refer to the ZO and CMP gathers. It can be seen as a decomposition of the travel-time squared $t(m,h)^2$ in terms of the squared ZO and CMP travel-times, $t(m,0)^2$ and $t(0,h)^2$, respectively. It is valid as long as the CRS travel-time approximation is. For example, it is exact for a dipping plane reflector with an homogeneous overburden.

We remark that a similar decomposition formula, using, however, travel-times instead of travel-times squared, have been presented in Tygel and Santos (2006), but it is valid in a shorter range.

Equation for amplitude

Although it has been relatively straightforward to predict the travel-time above, this is not the case with amplitude. This is so because CRS provides kinematic attributes only. As a matter of fact, full account of amplitudes involve many factors, such as angle-dependent reflection/transmission coefficients, geometrical spreading, medium attenuation, source wavelet, etc. Determination of all these quantities is, of course, unfeasible. Nevertheless, as shown below, a reasonable approximation can be achieved. Our idea is similar

to the one presented in a previous work by Rousset et al. (2001), that is to rely on the available data itself to estimate amplitudes.

We suppose we have full knowledge (traveltime and amplitude) at each sample of the two specific ZO and CMP gathers. More specifically, we consider that for each event that we select, the travel-time and amplitude pairs $(t(0,m), A(0,m))$ and $(t(0,h), A(0,h))$ that refer to the ZO and CMP gathers, respectively, are known. Note that, for the determination of the travel-time $t(m,h)$, we have already computed, with the help of the equations 4 and 5, the travel-times $t(m,0)$ and $t(0,h)$. We can therefore pick the corresponding amplitudes $A(m,0)$ and $A(0,h)$ within the given ZO and CMP gathers, together with the amplitude $A(0,0)$ at time $t(0,0)$ at the reference trace (see Figure 1). The question now is how to evaluate the unknown amplitude $A(m,h)$ relatively to these known (data-driven) quantities.

Our main assumption is that the predicted travel-time, $t(m,h)$, and amplitude, $A(m,h)$, are supposed to be valid only in the neighborhood around the reference trace, so the CRS travel-time equation should provide a good approximation. Concerning the amplitude, we further assume that the physical quantities such as velocities, densities, are also more or less stationary in this neighborhood. As a consequence, we may restrict the analysis to the main laterally variable factors, which are geometrical spreading and reflection angle. We propose here that the change of amplitude with offset (AVO effect) can be considered stationary with respect to midpoint variation. In this way, after estimating the amplitude change with offset at the reference point from the known CMP gather, we can use it as an estimate for amplitude change with offset for neighboring midpoints.

As the depth of the reflector can change laterally, it is clear that both the geometrical spreading and reflection angle can significantly change. In accordance, the changes in amplitude introduced by these two factors are investigated below.

- **Geometrical spreading:** As well known (see, e.g., Tygel et al., 1992; Červený, 2001), the precise evaluation of geometrical spreading can be a complicated task, with factors such as source and receiver ray angles, as well as second mixed derivatives of travel-time with respect of source and receiver coordinates. Once again, our goal here is to evaluate only the local change in geometrical spreading, in a "small" area where the earth subsurface is supposed to have stationary parameters. In this situation, we propose to approximate the change of geometrical spreading in terms of the variations in travel-time. More precisely, we will consider the change of amplitude as a function of the quantity $t(m,h)^\alpha$, namely the travel-time to the power α, where $\alpha = 1/2$ for the case of 2D in-plane spreading only and $\alpha = 1$ in the case of 3D spreading. We note, in particular, that for a planar dipping reflector in 2D with a homogeneous overburden, the geometrical spreading factor is exactly $t(m,h)^{1/2}$.

  From the above observations, we propose that, instead of trying to estimate the change in amplitudes, $A(m,h)$, we consider the change of the quantity $A(m,h).t(m,h)^\alpha$. This means that we consider the change in amplitude together with geometrical spreading variation. We also observe, in particular, that for the case of the above-described planar dipping reflector, the quantity $A(m,h).t(m,h)^{1/2}$ represents the so-called true amplitude, i.e., the amplitude after geometrical-spreading correction.

- **Reflection angle:** As the depth of the reflection point can vary with midpoint m, it implies that for a given half-offset h, the reflection angle, θ, can also vary with the reflection-time $t(m,h)$. Shuey (1985) has provided a useful approximation for the relative change with angle of the reflection coefficient, and therefore amplitude, that can be written in the form

$$R(\theta) - R(0) = A\sin^2(\theta) \tag{7}$$

  where $R(\theta)$ stands for the reflection coefficient as a function of the reflection angle, θ, and A is a constant that depends on the local physical parameters only. For our purposes, we can consider A as a constant in the neighborhood of the reference trace. Thus, the relative variation (ratio) of the reflection coefficient at any midpoint, m, with respect to the reflection coefficient at the reference midpoint can be simply approximated by the corresponding variation (ratio) of $\sin^2(\theta)$ at these two midpoints. We note, in particular, that for our familiar example of a planar dipping reflector in a 2D homogeneous overburden, this ratio can be shown to be equal to the ratio between squared travel-times.

Based on the above considerations, we propose to replace the variation of the quantity $R(\theta) - R(0)$ between midpoint m and the reference midpoint by the quantity $t(0,h)^2/t(m,h)^2$.

- **Final amplitude equation:** The two above considerations lead to the following equation to evaluate the amplitude at position, m, and half-offset, h,

$$A(m,h) = \frac{1}{t(m,h)^\alpha}\left\{A(m,0)t(m,0)^\alpha + [A(0,h)t(0,h)^\alpha - A(0,0)t(0,0)^\alpha]\frac{t(0,h)^2}{t(m,h)^2}\right\} \quad (8)$$

Note that this formula leaves unchanged the amplitude within the ZO gather ($h = 0$), as well as within the CMP gather ($m = 0$).

The evaluation of the unknown quantity, $A(m,h)$, relies only on quantities that are data-dependent, which can be picked from the two given specific configurations or computed from the CRS attributes. No other information is required, as long as the stationarity of model physical parameters in the vicinity of the reference position is a valid approximation. This process can therefore really be qualified as data-driven and macro-model-independent.

General Algorithm

We shall now assemble the above obtained results as building blocks of an algorithm that will produce a new data record at midpoint position, m, and half-offset, h (Figure 2), starting from the given ZO and CMP gathers in the neighborhood of the reference trace:

- First compute the CRS attributes for all samples of the record at the reference position ($m = 0$). For that, use the CMP gather (to obtain A_3 in the 2D case), and the ZO gather (to obtain A_1 and A_2 in the 2D case), together with the corresponding coherence values. This has to be done only once for all data traces to be built in the vicinity of the given reference trace.

- Start a loop on time samples, $t(0,0)$, with amplitude, $A(0,0)$, from the record at the reference midpoint, $m = 0$, and half-offset, $h = 0$. Each time sample will be taken as a possible reflection event if its CRS attributes have coherence values that are high enough. Otherwise, go to the next sample.

  - Compute $t(0,h)$, $t(m,0)$ and $t(m,h)$ from $t(0,0)$ and its CRS attributes, according to equations (4-6).
  - Pick $A(0,h)$ at time $t(0,h)$ in the CMP gather and $A(m,0)$ at time $t(m,0)$ in the ZO gather, using interpolation from surrounding data samples, and compute $A(m,h)$ using equation (8).
  - All obtained pairs of time and amplitude should be stored for future use. Note that calculated times are not necessary monotonously increasing. In the case there are more than one CRS groups of attributes for the same time sample (conflicting dips), this process has to be carried out for each CRS attribute group.

- End of the loop on time samples.

- Order the time-amplitude pairs by increasing times and interpolate the amplitudes at the data time-sampling rate.

The above algorithm, which builds a single data trace, can then be used in a loop on midpoint, m, and fixed half-offset, h, to build a common-offset (CO) section. In addition, in an outer loop on half-offset, h, it can be further used to build the full dataset.

Note that with this scheme, a given reflection event is built sample by sample, so that we do not have to make any assumptions on the signal wavelet, only that it has been adequately sampled. Preprocessing steps such as filtering or deconvolution that enhance the signal-to-noise ratio and signal resolution can be applied on the ZO and CMP gathers. This can be done either before or after the application of the algorithm.

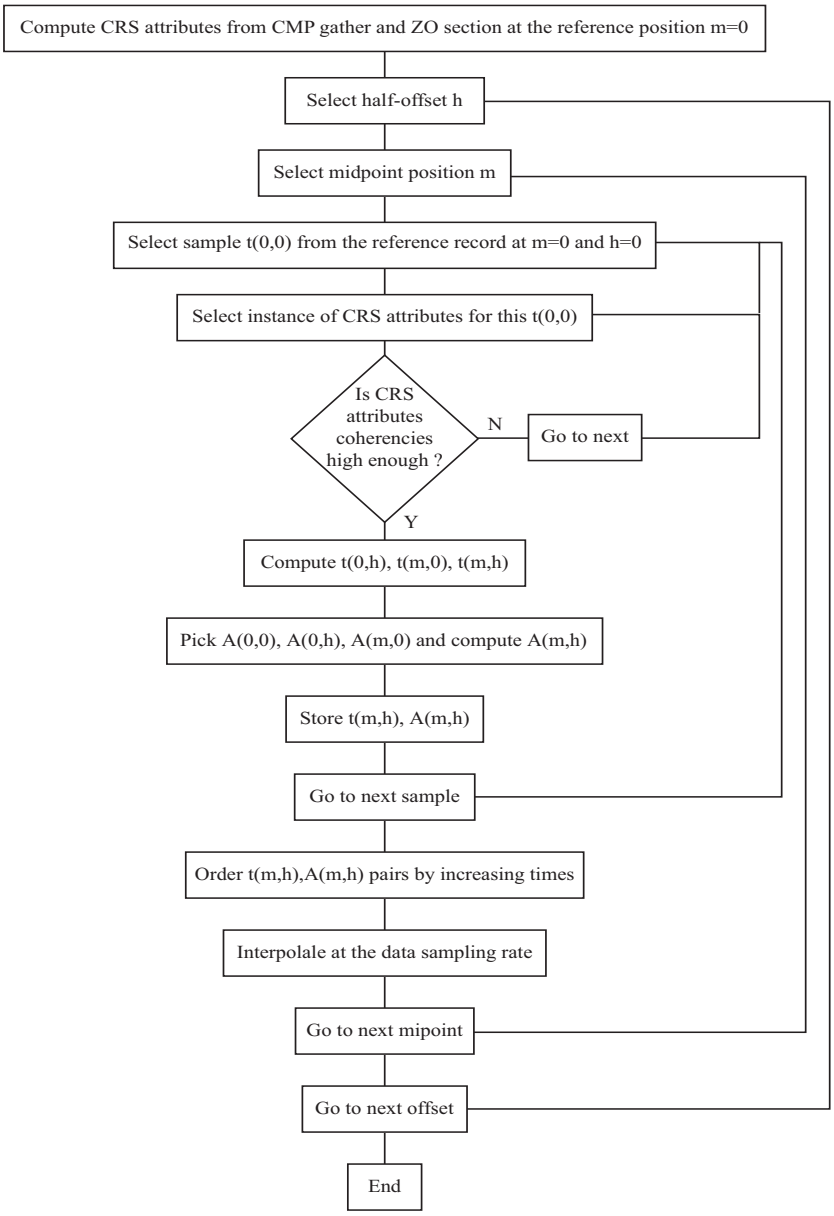

Figure 2: General algorithm to build data records from CRS attributes, ZO section and CMP gather

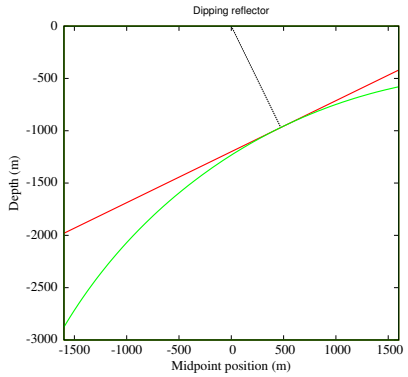

Figure 3: Simple synthetic examples: The red line represents the dipping planar reflector, the green line the circular reflector, and the black line the common normal ray, both reflectors being tangent at the normal incidence point

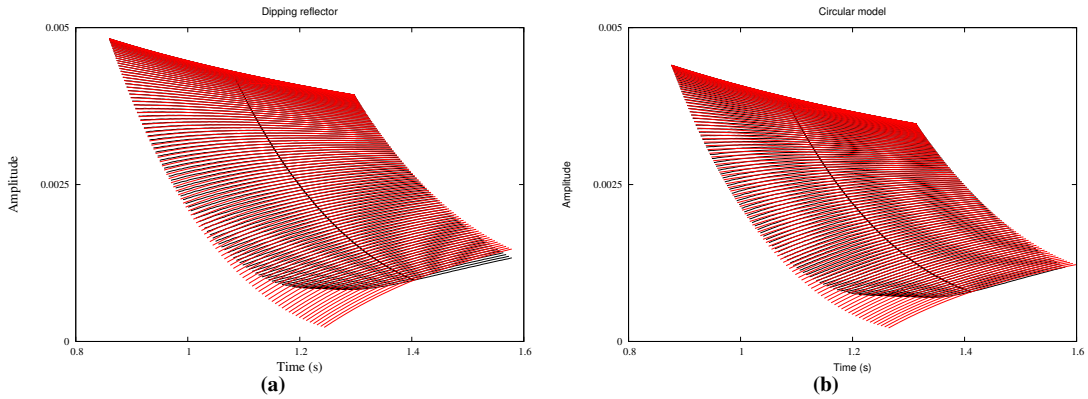

Figure 4: (a) Comparison of travel-time and amplitude along all CO sections between the theoretical values and the Inverse CRS equations, in the case of the dipping-planar reflector. The solid black lines represent the ZO and CMP sections where there are no differences; (b) Comparison of travel-time and amplitude along all CO sections between the theoretical values and the Inverse CRS equations, in the case of the circular reflector. Note the differences that now exist in both time and amplitude

SYNTHETIC EXAMPLES

The synthetic data have been computed by a ray-tracing calculation with 2D in-plane amplitudes, convolution by a ricker wavelet, and addition of white noise with a signal-to-noise ratio of 10.

Two simple models will be tested to check the efficiency of our algorithm. They are shown in Figure 3. The models consist of (1) a dipping planar reflector, within a homogeneous overburden, for which the time equation 6 is exact, and (2) a circular reflector, tangent to the dipping plane at the normal incidence point for the reference position, for which the time equation 6 is only approximate. The choice of these models reflects our assumption that the earth subsurface has to be locally simple enough so that the CRS travel-time equation provides a good approximation.

Dipping plane

Our first test was to compare the theoretical travel-time and amplitude values at any midpoint position, and offset, in the vicinity of the reference position, with the travel-time and amplitudes values obtained with equations 6 and 8, respectively. This comparison is shown in Figure 4(a), which reveals a very good agreement in most of the investigated range. The largest discrepancy arises for the lowest amplitudes.

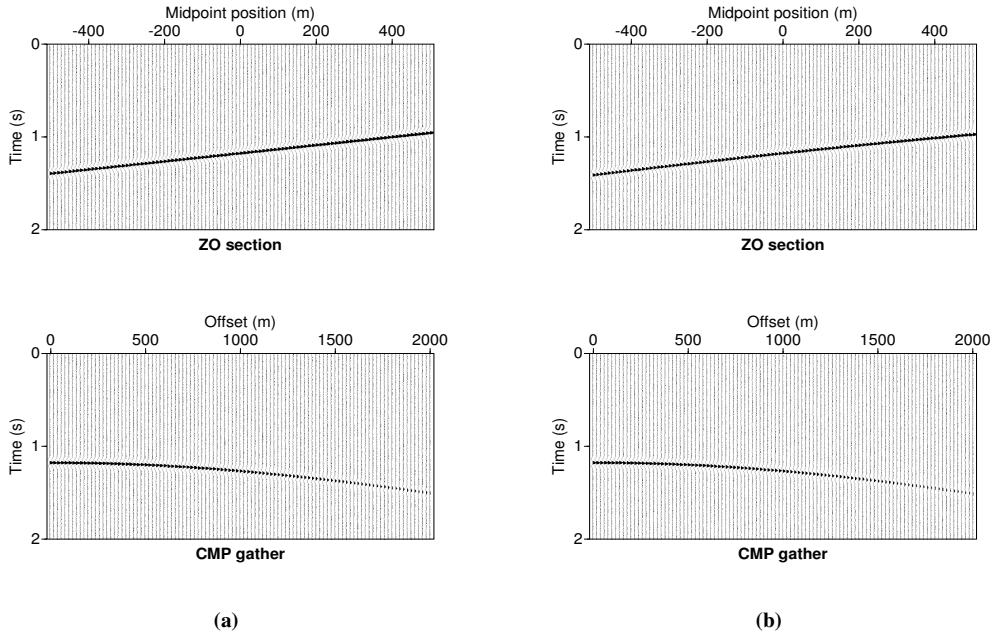

Figure 5: (a) Synthetic data for the planar dipping reflector; (b) Synthetic data for the circular reflector.

These correspond to largest offsets, as well as incidence angles close to the critical angle. Under this situation, the simple approximation we have used is not appropriate. However, the area where the two set of values can be considered very similar represents more than 90% of the full range. Note than in this case, the difference exists only in the amplitude value.

Figure 5(a) shows the two specific configurations that have been used to build the full dataset: the ZO gather on the top and the CMP gather at the bottom. From the traces in these two gathers, the CRS attributes at the reference midpoint $m = 0$ have been extracted, together with their coherence values. They are shown at Figure 6(a). Traces were then built following the algorithm shown in Figure 2, for all midpoints and offsets. The built traces are compared to the synthetic data in Figure 7(a), for small, medium and large offsets. We can see how the built trace compares well with the synthetic data in the vicinity of the reference midpoint, but differences appear when offset or distance to the reference midpoint increase. To evaluate how far we can go, a map of the relative mean quadratic error is shown in Figure 8(a). The contour at 0.2 provides a conservative estimation of the area where the approximation is very satisfying. It covers an extent approximately equal to the reflector depth, both in the offset and mid-point direction. Note that the noise is suppressed by the process when there is no coherent signal, that is when CRS attributes coherency is less than a given threshold.

Circular reflector

The same figures (Figure 4(b) to Figure 8(b)) were obtained for the circular reflector. Note that in this case, the CRS travel-time formula is only approximate, so the differences between the built traces and the synthetic data become significant for shorter offsets, or distances from the reference midpoint.

However, there further exists a significant range where the differences between the synthetic data and the data built with the Inverse CRS algorithm can be considered negligible. Its width, both in midpoint and offset coordinates are approximately equal to the target depth in these simple cases (about $1000m$). In order to check how the algorithm behaves in more complex situations, an illustration has been performed using real data.

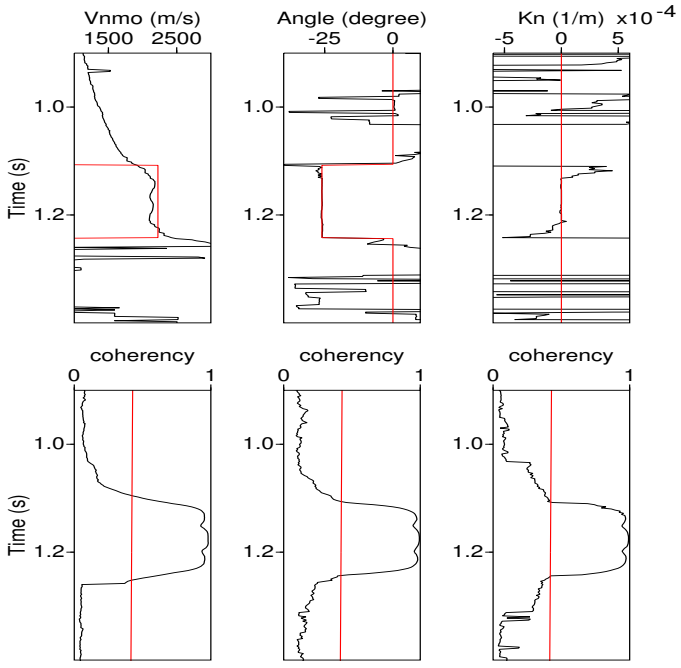

(a)

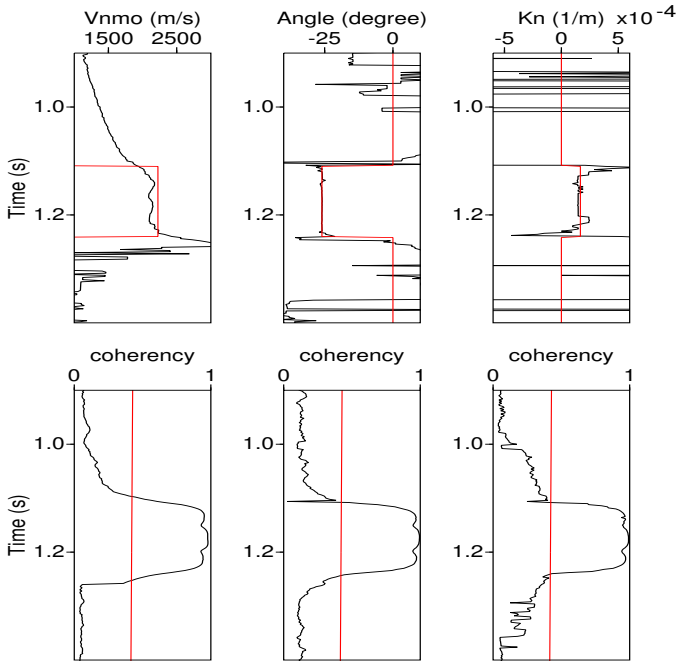

(b)

Figure 6: CRS attributes and their corresponding coherency obtained from the reference position. The expected attribute value in its validity range is also shown in red. The red line on coherency plots represents the coherency threshold for acceptance of attribute values: (a) Planar dipping reflector; (b) Circular reflector.

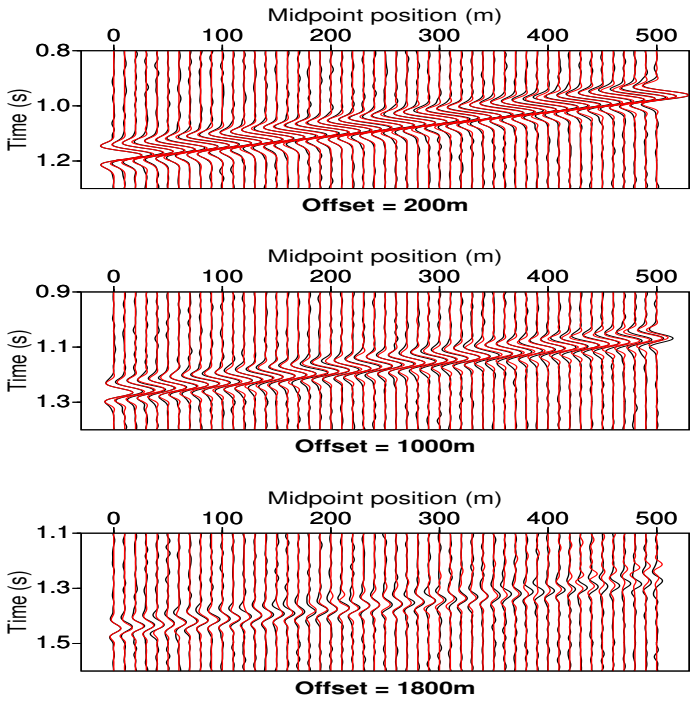

(a)

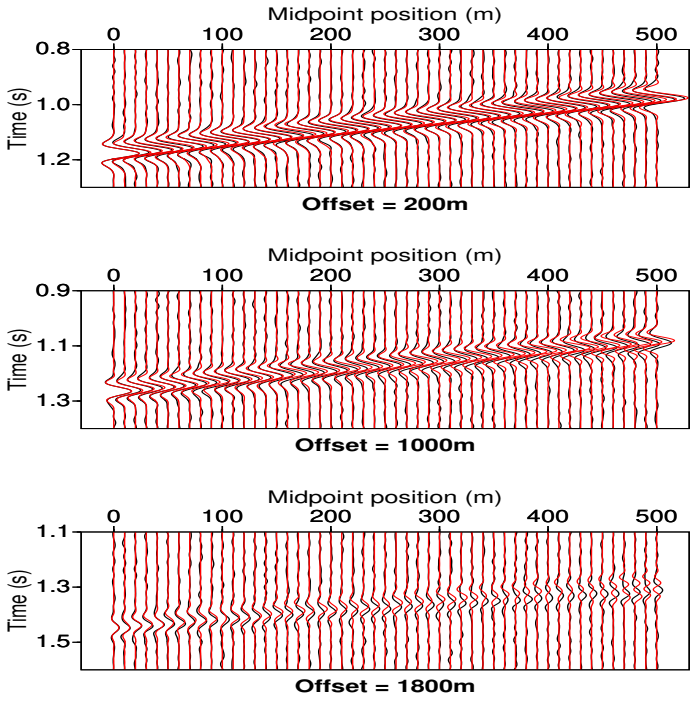

(b)

Figure 7: Comparison of the built traces with the synthetic data for small, medium, and large offsets, with the reference midpoint located at position 0: (a) Planar dipping reflector; (b) Circular reflector.

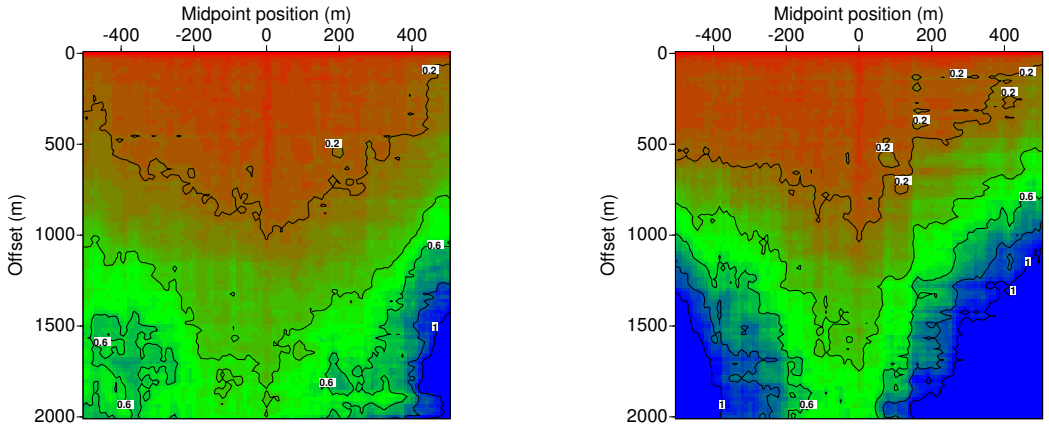

(a) **(b)**

Figure 8: Map of the relative mean quadratic error introduced by the process: (a) Planar dipping reflector; (b) Circular reflector.

REAL DATASET

In order to test the Inverse CRS algorithm in a real data case, we present an application for interpolating missing traces in a near-surface high-resolution seismic experiment, conducted in the alluvial plain of the river Gave de Pau, near Assat, southern France. As shown by the stack section obtained after conventional processing (Figure 9), the subsurface consists in a pile of horizontal depositional layers, with clear impedance contrasts at various times in the range $0.03-0.14s$, corresponding to depths between $30-150m$ for an average velocity around $2000m/s$. The data was obtained using $1m$ shot and trace intervals, and offsets in the range $0-70m$. To increase the CMP fold, neighboring CMP gathers were mixed 2 by 2, so the CMP interval is also $1m$. This stack section will be used here as our best estimate of the ZO section needed by the Inverse CRS algorithm.

The seismic acquisition experiment was conducted using a set of 2-channel DMT Summit boxes connected by a wire to the control unit. It appeared that one of the boxes was not working propery, so that the corresponding traces were killed for further processing. These missing traces are located in red in the acquisition map of Figure 10. Our purpose here will be to apply the Inverse CRS algorithm to build replacement traces, in order to avoid the processing artifacts generated by such discontinuities.

In order to apply the Inverse CRS algorithm, reference CMP gathers have to be chosen in the vicinity of the traces to be built. We present here the results corresponding to a set of demonstration gathers, which are shown in blue in Figure 10. The first one is the CMP gather corresponding to the CMP number 60, where three traces are missing. Next, two common offset gathers (COG) have been processed, corresponding to intermediate ($36m$) and large ($60m$) offsets. Two traces are missing in each of these gathers. The demonstration gathers are shown in Figure 11, with available traces in black. Note that noisy parts of the traces were muted both above and below the reflection events, to eliminate unwanted signals, such as refracted P-waves, or direct surface waves. Finally, reference CMP gathers, corresponding to CMP number 58 and 148, were chosen for Inverse CRS application. They are shown in green in Figure 10.

For the different demonstration gathers, the new traces, obtained using the Inverse CRS algorithm are shown in red in Figure 11, and compared with their normally acquired neighboring traces in black. In most cases, the results look very satisfying, especially when the offset is not too large. However, a few artifacts seem to appear in the COG $60m$: at the beginning of the unmuted zone, the offset is much larger than the target depth, so we should not expect the Inverse CRS approximations to be valid; at the end of the trace, the increase of the noise level seems to be responsible for the observed discrepancies. A somewhat unexpected good feature of the algorithm, is that it seems capable to reconstruct signals even in muted part

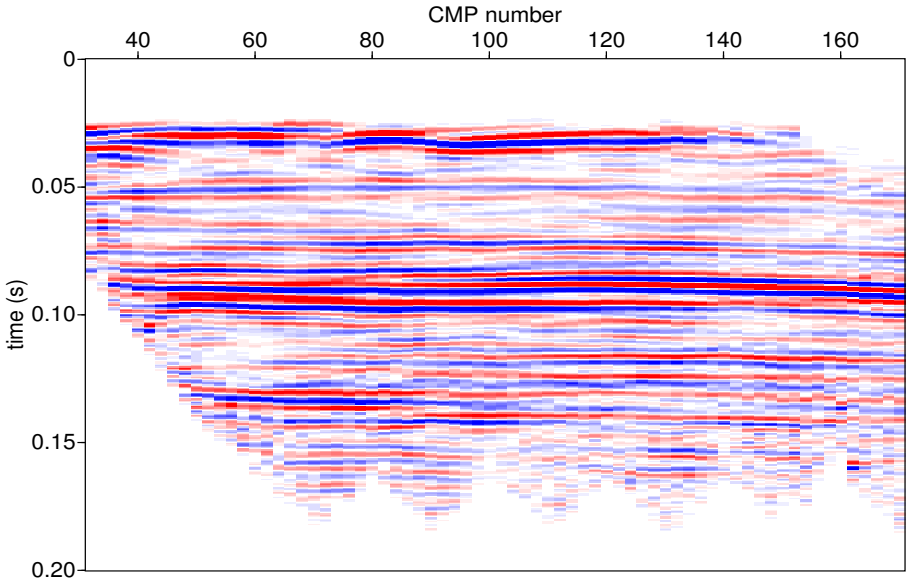

Figure 9: Conventional stack section, used here as the reference ZO section.

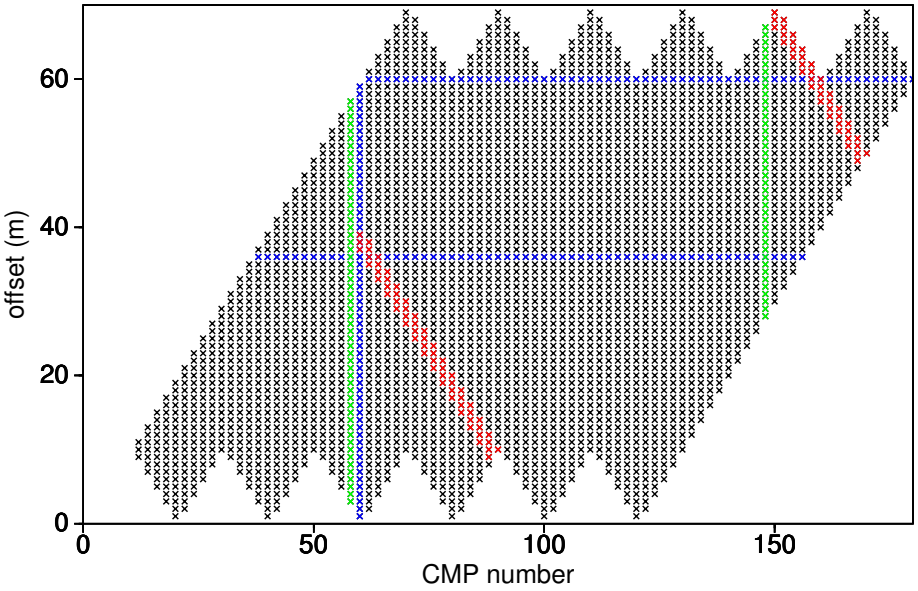

Figure 10: Acquisition map in the Offset-CMP coordinates, with missing traces in red, reference CMP gathers in green, and the gathers to be built in blue.

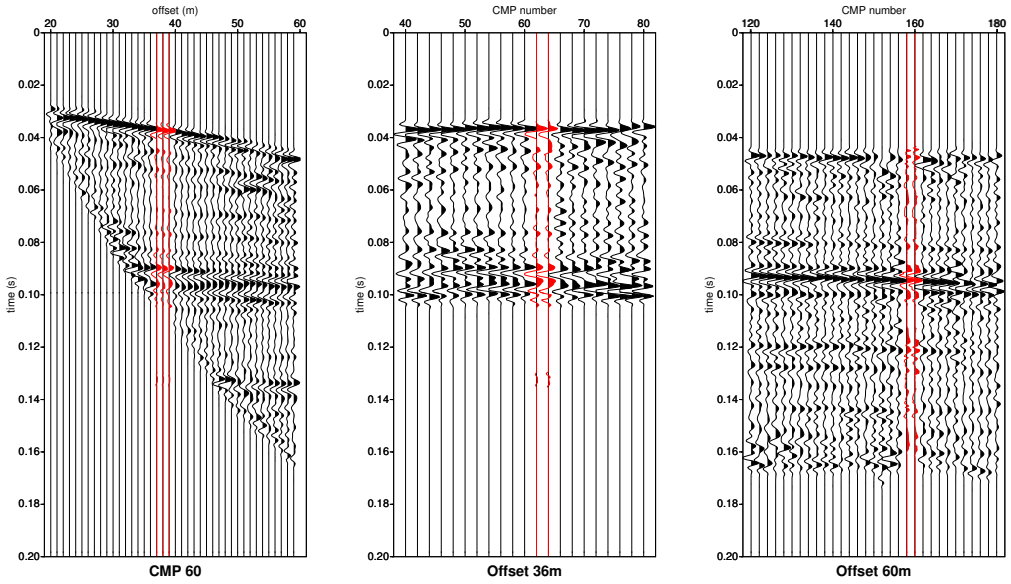

Figure 11: Results of the Inverse CRS traces building: the interpolated traces in red are compared with the normally acquired traces in black.

of the section. This can be seen by the event around $0.14s$, visible on the constructed traces, both in the CMP gather 60 and the COG gather $36m$.

CONCLUSIONS

At the present stage of this on-going research, we have proposed an algorithm that is able to build seismic traces from a very limited set of real data, namely a CMP gather and a ZO section, together with the CRS attributes that can be obtained from them. First synthetic tests of the algorithm provide satisfying results for the two simple cases of single dipping-plane and singular circular reflectors with a homogeneous overburden. The region of accepted approximations has been observed to be, in midpoint and offset, of a similar extent as the reflector depth in the first case, and a little less in the second case. Further tests carried out with real seismic data have also given positive results, showing the ability of the proposed algorithm to interpolate missing traces. Applications of this technique could be numerous, from noise suppression, data compaction, trace interpolation, etc...

ACKNOWLEDGMENTS

This research was initiated during the sabbatical stay of H.P. at the Laboratory of Computational Geophysics, State University of Campinas, Brazil, with the support of the Research Foundation of the State of São Paulo, Brazil). We acknowledge support of the National Council of Scientific and Technological Development (CNPq-Brazil) and from the sponsors of the WIT Consortium.

REFERENCES

Červený, V. (2001). Seismic ray theory. *Cambridge University Press.*

Della-Moretta, D., Klüver, T., and Marchetti, P. (2001). 3d CRS-based velocity model building - An accurate and cost-effective approach. *68th EAGE Conference and Exhibition, Vienna*.

Hubral, P. (1999). Special issue: Macro-model independent seismic reflection imaging. *Journal of Applied Geophysics*, 42:Nos. 3,4.

Jäger, R., Mann, J., Höcht, G., and Hubral, P. (2001). Common reflection surface stack: Image and attributes. *Geophysics*, 66:97–109.

Klüver, T. (2006). Velocity model building using migration to residual time. *76th SEG Annual Meeting, Ext. Abstr., New Orleans, USA*.

Koglin, I., Mann, J., and Heilmann, Z. (2006). CRS-stack-based residual static correction. *Geophysical Prospecting*, 54(06):697–707.

Perroud, H. and Tygel, M. (2005). Velocity estimation by the common-reflection-surface (CRS) method: Using ground-penetrating radar data. *Geophysics*, 70:B43–B52.

Prüssmann, J., Tygel, M., Gamboa, F., and Coman, R. (2006). Multiple suppression by the CRS technique. *GEO 2006, Bahrain*.

Rousset, D., Tygel, M., and Perroud, H. (2001). Attaching true amplitude to kinematically migrated images. *71st Ann. Internat. Mtg*, pages 292–295.

Shuey, R. T. (1985). A simplification of the Zoeppritz equations. *Geophysics*, 50(04):609–614.

Tygel, M. and Santos, L. T. (2006). Quadratic normal moveouts of symmetric waves in elastic media: A quick tutorial. *Studia Geophysica et Geodetica*, 51:185–206.

Tygel, M., Schleicher, J., and Hubral, P. (1992). Geometrical spreading corrections of offset reflections in a laterally inhomogeneous earth. *Geophysics*, 57(08):1054–1063.

Yilmaz, O. (2000). *Seismic Data Analysis*, volume 01, page 1000. Soc. of Expl. Geophys.